thus providing a microscopic explanation for the large critical current at matching magnetic fields.

REFERENCES AND NOTES

1. K. E. Osborne, *Philos. Magn.* **23**, 1113 (1971).
2. A. F. Mebard *et al.*, *IEEE Trans. Magn.* **1**, 589 (1977).
3. A. N. Lykov, *Solid State Commun.* **86**, 531 (1993).
4. V. V. Moshchalkov *et al.*, *Jpn. J. Appl. Phys.* **34**, 4459 (1995).
5. M. Baert *et al.*, *Phys. Rev. Lett.* **74**, 3269 (1995).
6. V. V. Metlushko *et al.*, *Solid State Commun.* **91**, 331 (1994).
7. C. P. Herring, *Phys. Lett.* **47A**, 105 (1974).
8. H. Dai *et al.*, *Science* **265**, 1552 (1994).
9. A. Bezryadin and B. Pannetier, *J. Low Temp. Phys.* **102**, 73 (1996).
10. S. Behler *et al.*, *Phys. Rev. Lett.* **72**, 1750 (1994).
11. L. N. Vu *et al.*, *Appl. Phys. Lett.* **63**, 1693 (1993).
12. K. Harada *et al.*, *Nature* **360**, 51 (1992).
13. J. E. Bonevich *et al.*, *Phys. Rev. Lett.* **70**, 2952 (1993).
14. T. Matsuda *et al.*, *Science* **271**, 1393 (1996).
15. K. Harada *et al.*, *Phys. Rev. B* **53**, 9400 (1996).
16. I. B. Khalfin and B. Ya. Shapiro, *Physica C* **207**, 359 (1993).
17. L. Radzihovsky, *Phys. Rev. Lett.* **74**, 4923 (1995).
18. E. Rosseel *et al.*, *Phys. Rev. B* **53**, R2983 (1996).
19. D. R. Nelson and V. M. Vinokur, *ibid.* **48**, 13060 (1993).
20. G. Blatter *et al.*, *Rev. Mod. Phys.* **66**, 1125 (1994).
21. It was pointed out by E. Zeldov that vortices were driven toward the center of the defect region by the force that was due to the Meissner current [E. Zeldov *et al.*, *Phys. Rev. Lett.* **73**, 1428 (1994)].

22. We thank N. Osakabe, T. Onogi, and R. Sugano of the Advanced Research Laboratory, Hitachi, Ltd., for discussions and comments; H. Hirose, H. Koike, and T. Ohnishi of the Instrument Division, Hitachi, and T. Kamino of Hitachi Instrument Engineering for assistance in operating the focused ion beam machine; F. Nagata and T. Shimotsu of Hitachi Instrument Engineering for discussion and electron microscopic observation; and S. Kubota, S. Matsunami, and N. Moriya of the Advanced Research Laboratory, Hitachi, for technical assistance in the experiment. V.V.M. acknowledges support from the Belgium Concerted Action (GOA) and National Fund for Scientific Research (NFWO) programs.

4 June 1996; accepted 6 September 1996

Human Influence on the Atmospheric Vertical Temperature Structure: Detection and Observations

Simon F. B. Tett,* John F. B. Mitchell, David E. Parker, Myles R. Allen

Recent work suggests a discernible human influence on climate. This finding is supported, with less restrictive assumptions than those used in earlier studies, by a 1961 through 1995 data set of radiosonde observations and by ensembles of coupled atmosphere-ocean simulations forced with changes in greenhouse gases, tropospheric sulfate aerosols, and stratospheric ozone. On balance, agreement between the simulations and observations is best for a combination of greenhouse gas, aerosol, and ozone forcing. The uncertainties remaining are due to imperfect knowledge of radiative forcing, natural climate variability, and errors in observations and model response.

There is considerable interest in the detection of a human influence on climate (*1*). Recent studies (*2*, *3*) have suggested that anthropogenic changes in greenhouse gases, sulfate aerosols, and stratospheric ozone (O_3) may have altered the vertical temperature structure of the atmosphere. In (*2*), simulations from several climate models were used to show that the pattern similarity between modeled and observed changes increased from 1963 to 1987. Several assumptions were made by Santer *et al.* (*2*): that the response to stratospheric O_3 changes can be added linearly to other responses, that the response of sea surface temperatures and clouds to O_3 changes can be ignored (*4*), that the lags between radiative forcing and climate response can be ignored, and that the response to forcings from different periods can be combined linearly.

We avoided making these assumptions by using time-dependent simulations from a single model including all the forcings. We extended the analysis to include the effect of the spatial mean as well as the patterns of change, and we extended the period considered to 1961 through 1995 by using a new radiosonde temperature data set. With less restrictive assumptions than those used in (*2*), we confirm that recent climate changes are unlikely to be entirely due to unforced climate variability. We show that our model is, on balance, in best agreement with the patterns and spatial means of recent climate change over this extended period when forced with a combination of increases in greenhouse gases and tropospheric sulfate aerosols, and stratospheric ozone loss.

Our model, HADCM2 (*5*), is a coupled atmosphere-ocean model with all components (ocean, atmosphere, and ice and land surface) having a horizontal resolution of 2.5° in latitude by 3.75° in longitude. The atmosphere has 19 levels, with 5 levels above 100 hPa, and the ocean has 20. Atmospheric temperature data were diagnosed on 15 pressure levels (*6*). To assess the significance of our results, we used data from 700 years of a control integration of HADCM2 where climate forcing was kept constant (*7*). The standard deviation (SD) of annual mean tropospheric temperature in this control simulation is similar to that observed (*7*), which gives some confidence in model estimates of natural variability.

Three different climate forcings (G, GS, and GSO) were used to force HADCM2. To reduce noise, we computed the responses to each forcing by averaging the responses from an ensemble of four simulations. Responses are identified by the name of the forcing used. The G and GS simulations were started from four states in the control integration separated by 150 years (*8*).

In G, HADCM2 was forced with an increase in equivalent CO_2, representing the effect of observed changes in all greenhouse gases, including CO_2, methane, and chlorofluorocarbons from 1860 to 1996 (*5*, *9*). In GS, HADCM2 was forced, in addition, with a simple parameterization of the effects of

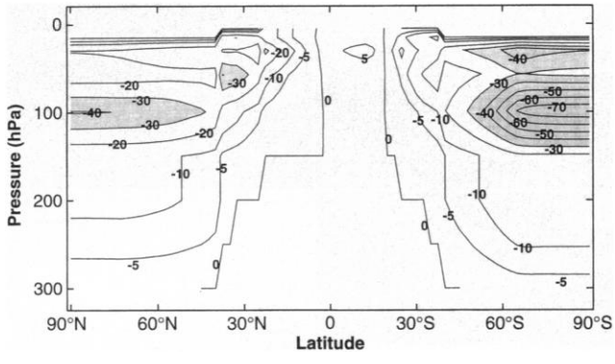

Fig. 1. Annual mean mass mixing ratio O_3 trends ($\times 10^9$) per year based on the use of a contour interval of 10×10^{-9} per year with extra contours at $\pm 5 \times 10^{-9}$ per year. Stippling shows where values are less than -30×10^{-9} per year.

S. F. B. Tett, J. F. B. Mitchell, D. E. Parker, Hadley Centre for Climate Prediction and Research, UK Meterological Office, London Road, Bracknell, Berkshire RG12 2SY, UK.
M. R. Allen, Space Science Department, Rutherford Appleton Laboratory, Chilton, Didcot, OX11 0QX, UK.
*To whom correspondence should be addressed. E-mail: sfbtett@meto.gov.uk

sulfate aerosols (*10*). In the G, GS, and control simulations, stratospheric O_3 remained constant (*11*).

Stratospheric O_3 has been observed to decrease, perhaps starting as early as the mid-1970s (*12*). Therefore, the forcing in GSO was identical to that in GS, except that after 1974 estimated changes in stratospheric O_3 were included and the simulations integrated to 1996. The largest annual mean O_3 losses occur at ~100 hPa over the polar regions (Fig. 1) (*13*). The GSO simulations were started from 1974 states in the GS simulations.

Zonal average, latitude pressure, temperature fields were computed from the responses of all three forced simulations and were compared with zonal means of a recently developed radiosonde temperature data set (*14*). In the simulations, unlike the observations, no data were missing. We computed signals, using these fields, by taking the difference between time means of the 10 years 1986 through 1995 and the 20 years 1961 through 1980 (Fig. 2). We compared these signals to equivalent calculations using the zonal-average estimates of the radiosonde observations.

All three forced simulations show similar large-scale responses, with cooling in the stratosphere, warming in the troposphere, and maximum warming in the upper tropical troposphere. The observations also show a pattern of tropospheric warming and stratospheric cooling but do not show the distinct equatorial upper tropospheric temperature maximum seen in the model simulations. The GSO signal shows greater cooling in the upper troposphere than the other simulations. Our signals show two main differences from those used by Santer *et al.* (*2*). First, the GS signal has much less hemispheric asymmetry than the equilibrium simulations shown by (*2*). This is due in part to the transient nature of the simulations, which gives less warming in the Southern Hemisphere. It is also due in part to the smaller, and probably more realistic (*15*), ratio of sulfate aerosol to greenhouse gas forcing used in GS (*16*) than by Santer *et al.* (*2*), resulting in less cooling in the Northern Hemisphere. Second, the GSO signal shows less tropospheric warming than the linear combinations of climate forcings and O_3 loss used by Santer *et al.* because in our simulations ocean temperatures respond to the forcing as a result of changes in stratospheric O_3.

The regionally averaged signals (Fig. 3) show the differences between the model simulations and the observations more clearly. The GSO simulation is in best agreement with the radiosonde observations in the upper troposphere–lower stratosphere but shows less warming than the other simulations and the observations in the lower troposphere. In extratropical regions, the GSO simulation shows less warming over all levels than the observations. In the tropics, all simulations show maximum warming at ~300 hPa, which is not seen in the spatially averaged observations and may therefore be due to model error.

There is a great deal of uncertainty in both the total and vertical distribution of O_3 loss. To give a crude estimate of the sensitivity of our results to this, we constructed a further signal (SENS1), which is the average of GSO and GS and, if we assume linearity, halves the effect of stratospheric O_3 (Fig. 3). We term the G, GS, GSO, and SENS1 signals forced signals.

To determine how similar the forced signals are to the observations, we used two measures of pattern similarity (*17*): (i) the weighted pattern correlation (R) (*18–20*) and (ii) the weighted congruence (g) (*18*). The correlation R is insensitive to the spatial mean changes, whereas g takes into account both the spatial mean and the pat-

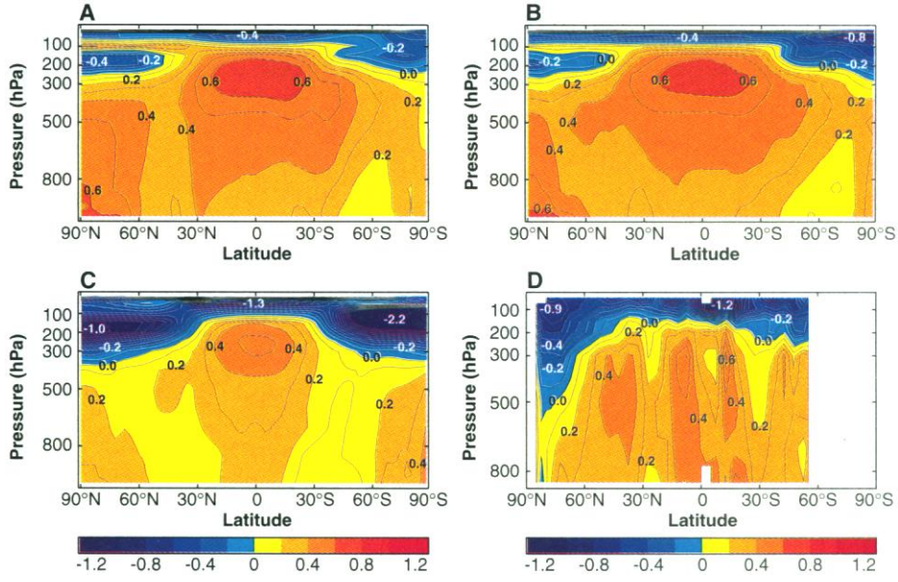

Fig. 2. Simulated and observed zonal mean temperature changes. (**A**) G signal; (**B**) GS signal; (**C**) GSO signal; and (**D**) observations. All signals are shown as a function of latitude and height and use a contour interval of 0.1 K. All signals are defined to be the difference between the decadal mean from 1986 through 1995 and the 20-year mean from 1961 through 1980.

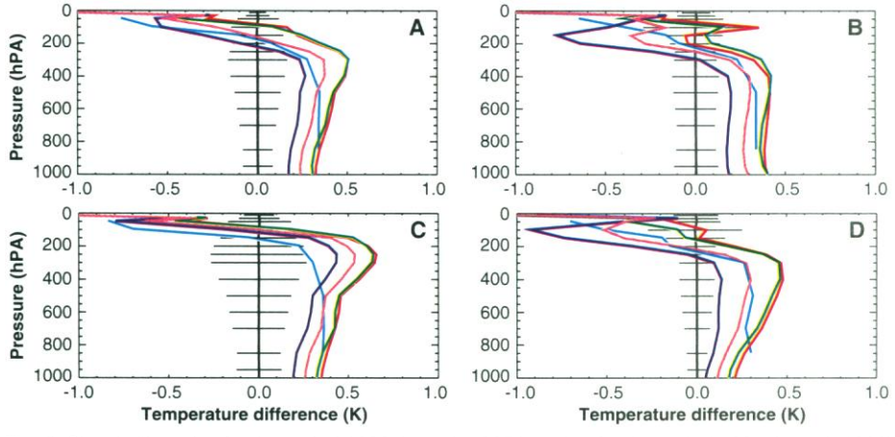

Fig. 3. Signals (the value for the period 1986 through 1995 less that for the period 1961 through 1980) averaged over four different regions. (**A**) Global (90°N to 90°S); (**B**) north extratropics (90°N to 30°N); (**C**) tropics (30°N to 30°S); and (**D**) south extratropics (30°S to 60°S). The horizontal lines about the zero line show ±1 SD for the control. Profiles are shown from the observations (light blue) and the G (red), GS (green), GSO (dark blue), and SENS1 (pink) signals. The uncertainty in the model signals, computed on the basis of a four-member ensemble, is ±1 control SD (we assume normally distributed noise). If the model variability is correct, the observed values have an uncertainty of ±2 SD.

tern (*20*). The closer R and g are to unity, the better the agreement. Two different weighting fields were used: mass weighting and volume weighting. Statistics computed on the basis of mass weighting are most sensitive to changes in the lower atmosphere, whereas statistics computed on the basis of volume weighting are most sensitive to changes in the upper atmosphere. We computed the values of g and R, using both weightings, from the observations and from each of the forced signals (Table 1).

To test the null hypothesis that the R and g values are due to unforced variability alone, we generated a population of 129 signals, from 700 years of the control integration (*21*). We computed R and g values between each of the forced signals and each of these control signals to give confidence intervals (*22*).

For all the simulations and SENS1, both R statistics have values greater than those obtained in any part of the control simulation (Table 1). Thus, in the entire 700 years of the control simulation no R statistic was ever as large as that computed between the observations and the forced simulations. If our estimate of unforced climate variability is correct, then unforced variability can be ruled out as a reason, with an estimated risk of error of ~2% (*22*), for the recent patterns of change in the vertical temperature structure of the atmosphere. In addition, the g statistics for the GSO and SENS1 signals are greater than those computed based on the control signals, suggesting that, for these forcings, agreement taking account of the spatial mean is greater than expected from unforced variability alone. In contrast, the g statistic for the G and GS signals is within that expected as a result of unforced climate variability. The significance is lower because the spatial means of both of these forced signals are warmer than the observations.

Next, we assessed which of the forced simulations is in best agreement with the observations. Because of unforced climate variability, we would not expect the simulations and observations to agree perfectly even if HADCM2 were perfect. Best agreement must be determined probabilistically: we asked, for two given simulations, what is the probability that R or g has a greater value in one simulation than the other? We computed the probabilities for pairs of forced simulations, using a bootstrap method (*23*, *24*) to take account of variability in both the observations and the ensemble mean signals (*25*).

For g, especially for the volume weighting, GSO is in significantly better agreement with the observations than either the GS or G simulations (Table 2, rows 1 and 2). For volume-weighted R, GSO is significantly worse than GS and G. This result suggests that the greatest impact of O_3 is to reduce the errors in the mean temperature, compared to the G and GS simulations (Fig. 3), while having little effect on, or even worsening, the pattern about the mean value.

Table 2, row 3, suggests that the GS signal is in slightly better agreement with the observed temperature changes than the G signal. The SENS1 signal is either significantly better than or not significantly different from either GSO, GS, or G on the basis of R and g (Table 2, rows 4, 5, and 6). On balance, out of all the signals considered, SENS1 is in best agreement with the observations.

Our results support the hypothesis of an anthropogenic effect on atmospheric vertical temperature structure as a result of the changing concentrations of greenhouse gases, stratospheric O_3 (probably weaker than in the GSO simulations reported here), and possibly sulfate aerosols since 1961. The comparison also acts as a model validation and increases the confidence in the ability of HADCM2 to predict future climate change.

There are several limitations in the current work. Agreement between the observations and forced simulations is only found on very large spatial scales, and all the simulations show too much upper tropospheric warming in the tropics. We have neglected possible natural external forcings, such as volcanic aerosols and changes in solar forcings, and also the effects of other anthropogenic forcings such as tropospheric O_3, nonsulfate aerosols, and the indirect effect of sulfate aerosols. There is uncertainty in the magnitude and distribution of the forcings caused by stratospheric O_3 and sulfate aerosols. It is likely that time-varying biases remain in the radiosonde data, especially in the stratosphere, and our work has taken no account of measurement uncertainty or measurement error. Finally, and most critically, our estimate of unforced variability is model-based and may be in error.

Table 1. Agreement, measured by pattern correlation (R) and congruence (g), between forced signals and observations based on the mass and volume weighting. We computed values using signals from each simulation (G, GS, and GSO) and the sensitivity study (SENS1). The maximum R or g value computed from 129 control signals with each forced signal is shown in parentheses. Where a value is greater (shown in bold) than the value in parentheses to its right, unforced climate variability is unlikely to be responsible for the agreement.

Signal	Mass weighting		Volume weighting	
	R	g	R	g
GSO	**0.73** (0.45)	**0.75** (0.43)	**0.75** (0.55)	**0.76** (0.45)
GS	**0.73** (0.43)	0.72 (0.81)	**0.81** (0.67)	0.60 (0.71)
G	**0.70** (0.46)	0.69 (0.84)	**0.81** (0.66)	0.51 (0.76)
SENS1	**0.75** (0.49)	**0.79** (0.68)	**0.80** (0.62)	**0.75** (0.58)

Table 2. Estimated risk of error for various statements (H_1). Values indicate the probability of observing the results obtained under the null hypothesis (H_0) that the statement (H_1) is false.

Statement	Mass weighting		Volume weighting	
	R	g	R	g
H_1: GSO better than GS	0.59	0.13	1.00†	0.00*
H_1: GSO better than G	0.19	0.01*	1.00†	0.00*
H_1: GS better than G	0.17	0.07	0.41	0.03*
H_1: SENS1 better than GSO	0.12	0.06	0.00*	0.65
H_1: SENS1 better than GS	0.23	0.00*	0.66	0.00*
H_1: SENS1 better than G	0.04*	0.00*	0.55	0.00*

*(†) indicate values at which H_0(H_1) may be rejected at the 5% level. Values of 0.00(1.00) are where the statement H_1 was never(always) rejected based on the limited number of independent R and g values (*22*) available.

REFERENCES AND NOTES

1. B. D. Santer, T. Wigley, T. Barnett, E. Anyamba, *Climate Change 1995: The Science of Climate Change* (Cambridge Univ. Press, Cambridge, 1996), chap. 8, pp. 407–444.
2. B. Santer *et al.*, *Nature* **382**, 39 (1996).
3. V. Ramaswamy, M. Schwarzkopf, W. Randel, *ibid.*, p. 616.
4. J. Hansen *et al.*, *Clim. Change* **30**, 103 (1995).
5. T. C. Johns *et al.*, *Clim. Dyn.*, in press.
6. Simulated temperature data exist at 1000, 950, 850, 700, 600, 500, 400, 300, 250, 200, 150, 100, 50, 30, and 10 hPa.
7. S. Tett, T. C. Johns, J. Mitchell, *Clim. Dyn.*, in press.
8. U. Cubasch *et al.*, *ibid.* **19**, 1 (1994).
9. J. F. B. Mitchell, T. C. Johns, J. M. Gregory, S. F. B. Tett, *Nature* **376**, 501 (1995).
10. J. F. B. Mitchell, R. A. Davis, W. J. Ingram, C. A. Senior, *J. Climate* **10**, 2364 (1995).
11. The O_3 data set is a seasonal climatology constructed from the zonal-mean climatology endorsed by the Commission Internationale pour la Recherche Atmosphérique (*26*) above 20 hPa and zonal-mean Solar Backscattered Ultraviolet satellite data for 1979 through 1981 (*27*) below 20 hPa.

12. A. J. Miller *et al.*, *Geophys. Res. Lett.* **19**, 929 (1992).
13. We computed stratospheric O_3 changes by first taking Total Ozone Measurement Satellite (*28*) trends for each 10° latitude band between 65°N and 65°S over the period 1979 to 1989 for each month. Poleward of 65°N and 65°S, the values at 65°N and 65°S were used. We converted the trends in total O_3 to trends in O_3 at each model level by assuming a constant percentage loss in the 7 km immediately above the tropopause (*3*). For the two model layers above this, we used a percentage loss rate of half that used in the lower layers. The position of the tropopause was defined from observed climatological average values. We computed the O_3 values by multiplying the trends by the number of years since 1974 and adding the result to the unperturbed values in (*11*).
14. The radiosonde data set is based on operationally received monthly averages, data from publications, data requested from national sources, and, for the South Pole, from the Comprehensive Aerological Reference Data Set (*29*). Data are for standard levels (850, 700, 500, 300, 200, 150, 100, and 50 hPa). Gross error and hydrostatic checks were applied (*30*). Comparisons with colocated Microwave Sounding Unit data since 1979 were used to assess and remove biases associated with recent instrumental changes at radiosonde stations operated by Australia and at some New Zealand stations. This reduced the cooling at 50 hPa since 1980 by about 2°C at some stations, with a noticeable impact on the Southern Hemisphere subtropical zonal average changes. The station data were gridded on a 5° latitude by 10° longitude grid as monthly anomalies (with respect to 1971 through 1990). Missing gridboxes were filled with the average of the anomalies in neighboring gridboxes, if at least three of these, out of a maximum of eight, had data. Unlike (*31*), no spatial interpolation was done. We converted the "filled" gridded data set to zonal monthly mean anomalies for each 10° latitude band at each pressure level by averaging with the requirement that there be at least 4 out of 36 longitude points present. If this was not the case, then for that latitude the zonal mean value was set to missing data. We converted the monthly average zonal mean anomalies to annual mean anomalies by averaging the 12 monthly values. At each latitude-pressure point, there must be at least 8 months with data; otherwise, the point was set to missing data in the annual mean.
15. K. P. Shine, Y. Fouquart, V. Ramaswamy, S. Solomon, J. Srinivasan, *Climate Change 1995: The Science of Climate Change* (Cambridge Univ. Press, Cambridge, 1996), pp. 108–118.
16. Over the period 1961 to 1995, in the HADCM2 simulations, the global mean forcing due to greenhouse gases increases by 1.5 W/m^2, whereas the negative global mean forcing due to tropospheric sulfate aerosols decreases by 0.23 W/m^2.
17. The pattern correlation (R) and the congruence (g) statistics are defined according to the following expressions:

$$R = \frac{\sum_{i,j} (M_{i,j} - \bar{M})(O_{i,j} - \bar{O})W_{i,j}}{\sqrt{\sum_{i,j} (M_{i,j} - \bar{M})^2 W_{i,j} \sum_{i,j} (O_{i,j} - \bar{O})^2 W_{i,j}}}$$

and

$$g = \frac{\sum_{i,j} M_{i,j} O_{i,j} W_{i,j}}{\sqrt{\sum_{i,j} M_{i,j}^2 W_{i,j} \sum_{i,j} O_{i,j}^2 W_{i,j}}}$$

where i and j are indices over latitude and pressure, $M_{i,j}$ is the model signal, $O_{i,j}$ designates the observed values, and $W_{i,j}$ is a weighting field. The spatial average, $\bar{F}$, for the model ($\bar{M}$) and the observations ($\bar{O}$) is

$$\sum_{i,j} F_{i,j} W_{i,j} \Big/ \sum_{i,j} W_{i,j}$$

Where, in either field, a data point was missing, that point was not included in the above computations. The weight arrays used are

$$\text{mass: } W_{i,j} = \cos \theta_i \tfrac{1}{2} (P_{j+1} - P_j)$$

$$\text{volume: } W_{i,j} = \cos \theta_i \tfrac{1}{2} (\log P_{j+1} - \log P_j)$$

where θ_i is the latitude and P_j is the pressure.
18. D. J. Karoly *et al.*, *Clim. Dyn.* **10**, 97 (1994).
19. B. D. Santer *et al.*, *ibid.* **12**, 77 (1995).
20. B. D. Santer, T. M. L. Wigley, P. D. Jones, *ibid.* **8**, 265 (1993).
21. Segments of zonal mean atmospheric temperature 35 years long were taken from the control integration. The start year of each segment was offset from the start year of the previous segment by 5 years giving a total of 129 segments. For each segment, means for years 1 to 20 (corresponding to 1961 through 1980 of the observations and forced simulations) and for years 26 to 35 (corresponding to 1986 through 1995 of the observations and forced simulations) were computed and differenced.
22. The R and g statistics computed between the control and forced signals have an estimated 70 to 80 degrees of freedom (*32*). Thus, a conservative estimate of the significance level of statistics greater than the maximum control value is 2%.
23. B. Efron and R. J. Tibshirani, *An Introduction to the Bootstrap* (vol. 57 of Monographs on Statistics and Applied Probability, Chapman and Hall, New York, 1993).
24. W. H. Press, S. A. Teukolsky, W. T. Vetterling, B. P. Flannery, *Numerical Recipes in Fortran: The Art of Scientific Computing* (Cambridge Univ. Press, Cambridge, ed. 2, 1992).
25. For each of the four forced signals and four statistics, we generated a probability distribution function (PDF) by (i) perturbing both forced simulations and observations by adding randomly selected segments of the control; (ii) computing trend patterns and four-member ensemble averages as before; (iii) computing R and g statistics between perturbed patterns; and (iv) repeating 2500 times to build a PDF. The resulting PDFs of R and g are non-Gaussian and biased with respect to the unperturbed values due to the normalization. This can be understood if one considers two patterns (P_1, P_2) that are perfectly correlated ($R = 1$). Adding noise to P_1 will reduce the correlation to less than 1. We correct with a Fisher z transformation (*24*), translating the transformed PDFs such that their average values are equal to the transformed values obtained with the unperturbed signals. Results in Table 2 are then computed directly from these transformed PDFs. We believe that the bias correction gives the most accurate risk estimates. Use of it does not affect our key result that SENS1 is, on balance, in best agreement with the observations.
26. G. Keating, D. Young, M. Pitts, *Adv. Space. Res.* **7**, 105 (1987).
27. D. Heath, P. K. Bhartia, R. D. McPeters, *J. Geophys. Res.* **89**(D4), 5199 (1984).
28. *Tech. Rep. 37* (Word Meteorological Organization, Geneva, 1994).
29. R. E. Eskridge *et al.*, *Bull. Am. Meteorol. Soc.* **76**, 1759 (1995).
30. D. E. Parker and D. I. Cox, *Int. J. Climatol.* **15**, 473 (1995).
31. A. H. Oort and H. Liu, *J. Climate* **6**, 292 (1993).
32. F. W. Zwiers and H. von Storch, *ibid.* **8**, 336 (1995).
33. T. Johns carried out the G and GS ensemble simulations. D. Sexton and D. Karoly produced the O_3 data set, using data provided by K. Shine. M. Gordon, D. Cullum, and M. O'Donnell carried out much of the processing required to produce the radiosonde data set. The work was partially supported by the U.K. Department of the Environment under contract PECD 7/12/37 (S.F.B.T., J.F.B.M., D.E.P., and computer time) and the U.K. Natural Environment Research Council and Wolfson College, Oxford (M.R.A.).

5 June 1996; accepted 26 September 1996

Dynamics of Oxidation of a Fe^{2+}-Bearing Aluminosilicate (Basaltic) Melt

Reid F. Cooper,* John B. Fanselow, J. K. Richard Weber†, Dennis R. Merkley, David B. Poker

Rutherford backscattering spectroscopy (RBS) and microscopy demonstrate that the ~1400°C oxidation of levitated droplets of a natural Fe^{2+}-bearing aluminosilicate (basalt) melt occurs by chemical diffusion of Fe^{2+} and Ca^{2+} to the free surface of the droplet; internal oxidation of the melt results from the required counterflux of electron holes. Diffusion of an oxygen species is not required. Oxidation causes the droplets to go subsolidus; magnetite (Fe_3O_4) forms at the oxidation-solidification front with a morphology suggestive of a Liesegang-band nucleation process.

The structure and dynamics of silicate melts are first-order dependent on the valence state of incorporated transition metal cations, particularly, in the case of geological melts, iron (*1*, *2*). As a consequence, understanding the chemical diffusion process by which a melt comes into redox equilibrium with its environment is critical in characterizing its structural and chemical evolution. Diffusion studies have emphasized two approaches: (i) oxygen (^{18}O) tracer diffusion experiments [for example, (*3*, *4*)] and (ii) transition-metal-cation redox experiments, which are analyzed based on the assumption that diffusion of an oxygen species dominates the redox kinetics [for example, (*5*–*7*)]. There is a noted discrepancy between the

R. F. Cooper and J. B. Fanselow, Departments of Materials Science and Engineering and Geology and Geophysics, University of Wisconsin–Madison, 1500 Engineering Drive, Madison, WI 53706, USA.
J. K. R. Weber and D. R. Merkley, Intersonics Incorporated, 3453 Commercial Avenue, Northbrook, IL 60062, USA.
D. B. Poker, Oak Ridge National Laboratory, Mail Stop 6048, Post Office Box 2008, Oak Ridge, TN 37831, USA.
*To whom correspondence should be addressed.
†Present address: Containerless Research, Inc., 910 University Place, Evanston, IL 60201, USA.